# EFFECTS OF GRAVITY ON SHEARED TURBULENCE LADEN WITH BUBBLES OR DROPLETS

Said Elghobashi[1], [1]Mechanical and Aerospace Engineering Department, University of California, Irvine, California 92697, USA, selghoba@uci.edu, Juan Lasheras[2], [2] Applied Mechanics and Engineering Sciences Department, University of California, La Jolla, California 92093, USA, lasheras@ames.ucsd.edu

## 1 INTRODUCTION

The objective of this numerical/experimental study is to improve the understanding of the effects of gravity on the two-way interaction between dispersed particles (bubbles or liquid droplets) and the carrier turbulent flow. Due to the imposed page limit, only a condensed description of the results will be presented. Reference is made to other publications for the details.

The experiments reported here are concerned with the dispersion of liquid droplets by homogeneous turbulence under various gravitational conditions and the effect of these droplets on the evolution of the turbulence of the carrier fluid (air).

The numerical results presented here are obtained from direct numerical simulations (DNS) of bubble - laden turbulent flow to examine the effects of small bubbles on the behavior of decaying turbulence. All published DNS studies of turbulent flows laden with particles, except [7], adopt the Lagrangian-Eulerian approach. In this approach the carrier flow velocity field is obtained by solving the Navier-Stokes and continuity equations at fixed mesh points whereas the trajectories of the dispersed particles are computed by solving the Lagrangian equation of particle motion [1],[2]. Using this method to simulate turbulent flows with two-way coupling between the particles and the carrier flow is limited at present and in the foreseeable future by the memory and speed of available supercomputers, including the latest parallel supercomputers. This limitation forces all DNS of particle - laden turbulent flows (with two-way coupling) to compute the trajectories of *only* a fraction of the *actual number* of particles. The accuracy of DNS results is directly proportional to the magnitude of this fraction, being highest when the fraction equals unity [2].

The alternative approach for predicting particle-laden flows is known as the 'two-fluid' (TF), or 'Eulerian-Eulerian', approach [3], and has been used only with the Reynolds - averaged equations of motion, not with DNS. In the TF approach, the governing equations are obtained by volume - averaging the equations of motion of both phases (the carrier flow and particles) based on the assumption that the dispersed particles behave as a "continuum" under certain conditions.

The objective of the numerical part of this paper is to describe briefly how DNS can be performed using the two-fluid approach for bubble - laden homogeneous isotropic turbulence without forcing. More details are given in [7]. Turbulent homogeneous shear flows laden with droplets/bubbles will be studied in the next phase of the project.

## 2 NUMERICAL STUDY

### 2.1 Governing Equations

We consider spherical bubbles with diameter $d$ much smaller than the characteristic length scale of the flow, $L_f$, and average the equations of motion of the fluid and bubble over a length scale scale $\lambda$ which is much smaller than $L_f$ but much larger than the bubble diameter, $d \ll \lambda \ll L_f$. Thus the bubble phase can be treated as a continuum characterized by the velocity $V_i(\mathbf{r},t)$ and concentration (or, volume fraction) $C(\mathbf{r},t)= \pi d^3 n(\mathbf{r},t)/6$, where $n(\mathbf{r},t)$ is the bubble number density.

We assume that the density of the gas and, consequently, the mass of the bubble are negligible compared to those of the surrounding fluid, $\rho_f \gg \rho_b = 0$. We also assume that the bubble concentration, $C$, is small enough (i.e. $C \leq 10^{-3}$) and thus neglect its contribution to the fluid inertia and continuity, i.e. we retain $C$ only in the buoyancy term in the momentum equation of the carrier flow. This is analogous to the Boussinesq approximation in a stratified fluid with effective density $(1-C)\rho_f$.

The resulting equations of the conservation of the fluid and bubble phase momentum and mass are [7]:

$$\frac{DU_i}{Dt} = -\frac{1}{\rho_f}\partial_i \tilde{P} + \nu \Delta U_i + (C - < C >)\, g\, \delta_{iz}\,, \quad (1)$$

$$\partial_j U_j = 0\,, \quad (2)$$

$$\frac{dV_i}{dt} = 3\frac{DU_i}{Dt} + \frac{1}{\tau_b}(U_i - V_i + W\delta_{iz})\,, \quad (3)$$

$$\frac{\partial C}{\partial t} + \partial_j C V_j = 0\,, \quad (4)$$

where $U_i$ is the fluid velocity, and $V_i$ is the velocity of the bubble phase. The Lagrangian derivatives $D/Dt = \partial/\partial t + U_j\partial_j$ and $d/dt = \partial/\partial t + V_j\partial_j$ are taken along the trajectories of the fluid point and bubble, respectively, and $g$ is the projection of the gravity acceleration on the $z-$ axis, $g_i = -g\delta_{iz}$. The modified hydrostatic part $\tilde{P}$ of the pressure field in eq.(1) is defined as:

$$\tilde{P} = P + \rho_f g \int_0^z (1 - < C >) dz \,, \tag{5}$$

where $< C >$ is the ensemble-averaged bubble concentration. We evaluate $< C >$ as an average over a horizontal (z) plane. The bubble response time $\tau_b$ and terminal velocity $W$ are defined as

$$\tau_b = \frac{d^2}{36\nu} \,, \tag{6}$$

$$W = 2\tau_b g \,. \tag{7}$$

The momentum conservation and continuity equations (1)-(4) for both phases are solved in a cubical domain with periodic boundary conditions. The equations are discretized in an Eulerian framework using a second-order finite-difference technique on a staggered grid containing $96^3$ points equispaced within unit length in each of three coordinate directions (x,y,z). The Adams - Bashforth scheme is used to integrate the equations in time. Pressure is obtained by solving the Poisson equation using Fast Fourier Transform. More details about the numerical method and its accuracy are discussed by Elghobashi and Truesdell [6].

## 2.2 Results

In this section we present the DNS results for bubble dispersion in isotropic decaying turbulence with both one-way and two-way coupling.

### 2.2.1 Dispersion of bubbles in isotropic decaying turbulence (with one-way coupling)

DNS of bubble dispersion in isotropic decaying turbulence is performed with the initial condition: $Re_{\lambda 0} = 25$. The initial bubble velocity and concentration are prescribed as:

$$V_i = \delta_{iz} W, \;\; C_0 = \alpha_0 \,, \tag{8}$$

where the bubble terminal velocity $W$ is given by (7).

The ability of the simulation to resolve the motion at the smallest turbulence scales is assured by the criterion $\eta\, k_{max} > 1$, where $k_{max}$ is the highest resolved wavenumber, and $\eta$ is the Kolmogorov length scale $\eta = (\nu^3/\epsilon)^{1/4}$. The bubble response time is restricted by the two conditions :

$$d_b < \eta \,, \tag{9}$$

$$Re_b = \frac{W\, d_b}{\nu} < 1, \tag{10}$$

which are necessary for the derivation of (3) [7]. Substituting the terminal velocity (7) and the bubble diameter ($d_b = (36\nu\tau_b)^{1/2}$) in (9) and (10), and using the equality $\eta^2 = \nu\tau_k$, we rewrite the conditions (9) and (10) respectively as

$$\frac{\tau_b}{\tau_k} < \frac{1}{36} \simeq 0.028, \tag{11}$$

$$\tau_b < \left(\frac{\nu}{144 g^2}\right)^{1/3} = \tau_* \,. \tag{12}$$

Both conditions (11) and (12) are satisfied throughout our simulations.

Figure 1 shows the time evolution of the concentration spectrum. It is evident that no numerical instability occurs. The spectrum $E_C(k)$ at high wave numbers approaches an asymptotic form at t=10. The high wavenumber range in the spectrum (i.e. $k \geq 40$) would detect any numerical instability if it existed. The reason for the absence of the instability is that the fluctuations of the bubble concentration, caused by the preferential accumulation, are proportional to the ratio $\tau_b/\tau_k$ which decreases with time (approximately as $\sim 1/t$) in decaying turbulence.

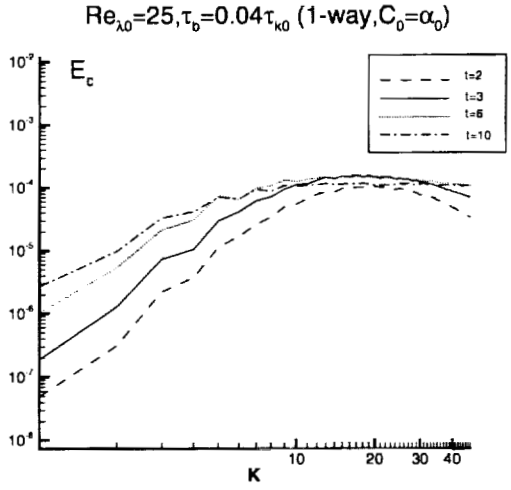


Figure 1: Time evolution of spectrum of bubble concentration fluctuation

It should be noted that both the accumulation of bubbles and the absence of the diffusivity in the transport equation for the bubble concentration (4) may lead to instabilities in the numerical solution due to the development of steep gradients in the concentration field. The occurrence of this numerical instability depends on the initial distribution of the bubble concentration, the flow Reynolds number and the bubble response time. In our DNS we chose the initial microscale Reynolds number $Re_{\lambda 0} = 25$, so that at time of the injection of bubbles (t=1) the small-scale motions are resolved, i.e. $k_{max}\eta \geq 1$ where $k_{max} = N_g\pi$ is the maximum wave number for the given grid resolution $N_g = 96$. The numerical instability may occur for higher-inertia bubbles, i.e. for $\tau_b$ of the order of the Kolmogorov time scale $\tau_k$. However, prescribing $\tau_b \simeq \tau_k$ would violate the condition $d_b < \eta$, which is necessary for deriving equation (3) of bubble motion.

## 2.3 Two-way coupling effects on decaying turbulence

Here we examine the effects of the dispersed bubbles on the temporal development of decaying isotropic turbulence. We consider three cases with different initial bubble concentration profiles in z-direction, but with the same bubble response time as in the one-way coupling case.

The first case is for a uniform initial bubble concentration, $C_0 = \alpha_0$, where $\alpha_0$ is a reference concentration set equal to 0.005 to allow neglecting bubble-bubble interactions. The second case is for stable linear stratification, with a constant concentration gradient in the vertical (z) coordinate, $C_0 = \alpha_0(1 + z)$, while the third case is for unstable linear stratification, $C_0 = \alpha_0(2 - z)$. In the cases of stable and unstable stratification, periodic boundary conditions in the z-direction are imposed on the instantaneous concentration fluctuation $C' = C - < C >$. We first consider the modification of the turbulence energy spectrum $E(k)$, which is governed by

$$\partial_t E(k) = T(k) - \epsilon(k) + \Psi_b(k), \qquad (13)$$

where $\epsilon(k)$ is the dissipation rate of $E(k)$, and $T(k)$ is the rate of energy transfer between the wave numbers (i.e. between the different scales). The source of the modification of the energy spectrum and spectral transfer process is $\Psi_b(k)$ which can be regarded as a spectral buoyancy flux, analogous to that in a stratified fluid with density $C'$, and is defined as

$$\Psi_b(\boldsymbol{k}) = g\, Re\, \{C'(\boldsymbol{k})U_z^*(\boldsymbol{k})\}\,. \qquad (14)$$

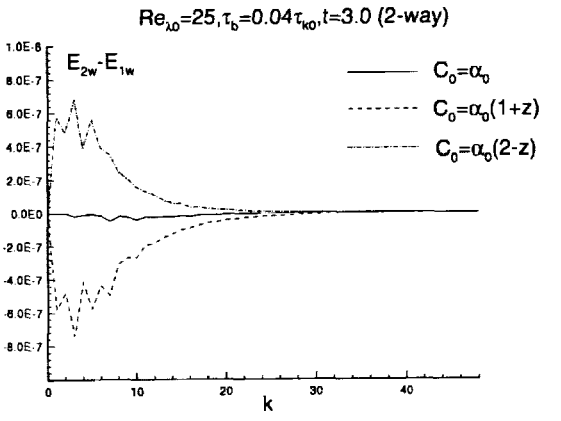


Figure 2: Modification of the turbulence energy spectrum in a bubble-laden decaying turbulence

Figure 2 shows the difference between the energy spectra in two-way and one-way coupling cases computed at time t=3. As expected, the turbulence energy increases in the case of unstable stratification and is reduced in the case of stable stratification. In the non-stratified two-way coupling case, the spectrum remains practically unchanged compared to the one-way coupling case.

# 3 EXPERIMENTAL STUDY

The objectives of the experiments reported here are measuring the dispersion of the droplets by homogeneous turbulence under various gravitational conditions and determining the effects of the presence of the droplets on the evolution of the turbulence of the carrier fluid (air).

**Experimental facility and initial conditions**

The experimental facility (Fig. 3) consists of a blow-down wind tunnel made up of two sections. The first section serves as the two-phase flow generation system, while the second is a 2 meter long test section of $20 \times 20\,cm$ square cross section. The air flow, which is supplied by a blower, passes through a slight contraction duct followed by a honeycomb and a grid which damp out the fluctuations generated by the blower. The air stream then flows through the spray generation system. This system consists of two arrays of 33 airblast atomizers each arranged so that the air flow is uniformly laden with droplets. Each atomizer is made of a pressurized

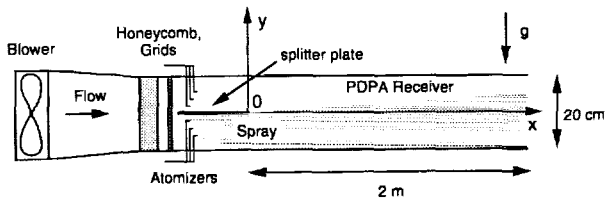


Figure 3: Experimental facility.

air jet impinging normally onto a water jet, thus creating a spray whose main characteristics are given by the pressure of the air and the water flowrate supplying the liquid jet [10],[11]. In the experiments reported here, only one of the two arrays was supplied with water, thus only half of the cross section of the channel flow was loaded with droplets. A splitter plate is placed horizontally at the mid-plane of the channel, separating the droplet-laden flow from the non laden air flow (see Fig. 3). The length of the splitter plate is long enough to ensure that the size distribution of the droplets is uniform across the cross section of the channel before entering the test section. Note that $x$, $y$, $z$ correspond respectively to the longitudinal, normal and spanwise coordinates. Due to the spanwise uniformity of the flow, all measurements reported here were made at the $z = 0$ plane.

Preliminary measurements have been carried out to determine the characteristics of both the turbulent air flow and the spray. Velocity measurements were made using hot-wire anemometry. Measurements of mean longitudinal velocity profiles show that the small wake resulting from the presence of the splitter plate follows the common decay law $\frac{\Delta U}{U} \propto x^{-1/2}$, where $\Delta U$ is the velocity deficit in the wake. Since for $x > 35\,cm$, $\frac{\Delta U}{U} < 10\%$, most of the measurements reported here have been done beyond this downstream location where it is then considered that the wake has no longer influence on the flow. As we are interested in the interaction between the particules and a homogeneous turbulent flow, we restricted our investigation to the region $-40\,mm < y < 40\,mm$ in order to avoid any effect of the boundary layers forming at the top and bottom surfaces of the test section. The mean velocity in the free stream selected for these experiments, $U$, is $14\,m/s$, while the longitudinal turbulent intensity , $u'/U$ is measured to be $2\%$. This corresponds to mean and turbulent Reynolds numbers, $Re = \frac{UH}{\nu}$ and $Re_t = \frac{u'L}{\nu}$, of $1.9\,10^5$ and 1900 respectively. $H$ is the height of the channel, and $L$ is the integral scale of the flow, calculated from the turbulent spectrum measured in the free

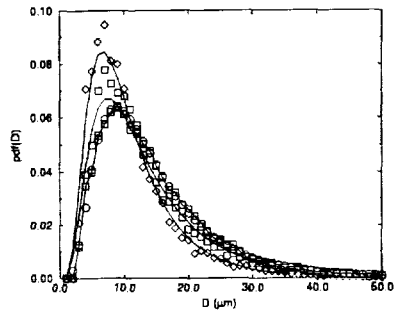


Figure 4: Probality density function for ○, $y = -30$; □, 0; ◇, 30 mm, — respective log-normal fits, x=19 cm, stable stratified case.

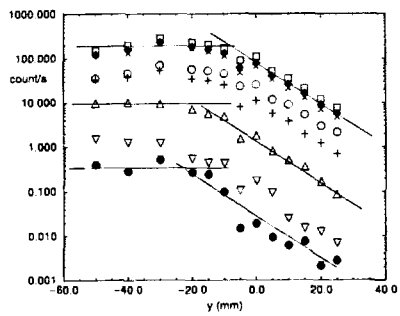


Figure 5: Flux of particles profiles, x=107 cm. ○, $D < 5$; □, 10; ◇, 15; ×, 25; +, 35; △, 50; ▽, 65; •, 80 $\mu m$.

stream. It is approximately $10\,cm$. The droplet void fraction in the free stream is $\alpha = 1.8\,10^{-5}$. The spray size distribution and the velocity of the droplets were measured with a Phase Doppler Particle sizer (Aerometrics PDPA). This instrument has already been tested successfully on a similar experiment [9]. The initial size distribution is shown in Fig. 4 by the open circles. The corresponding mean size is $D_{10} = 15\,\mu m$ and the Sauter Mean Diameter is $D_{32} = 33\,\mu m$. As can be seen, the initial probability density function for the droplet sizes is well described by a log-normal distribution. As we are interested in determining the turbulent diffusivity of the droplets of various sizes, velocity measurements and concentration of droplets have been done for different sizes of particles. For this purpose, PDF have been discretized into 8 bins corresponding respectively to diameters, $D$, less than 5, 10, 15, 25, 35, 50, 65 and 80 $\mu m$.

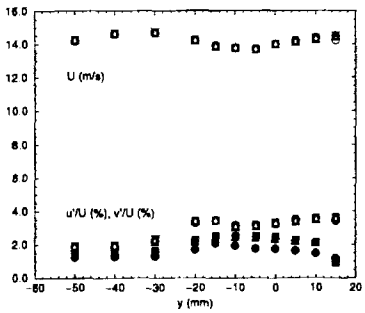


Figure 6: Mean and fluctuations velocity profiles, x=67 cm. Open symbols, longitudinal velocity; closed symbols, normal velocity. ○, $D < 5$; □, 15; ◇, 35; △, 80 $\mu m$

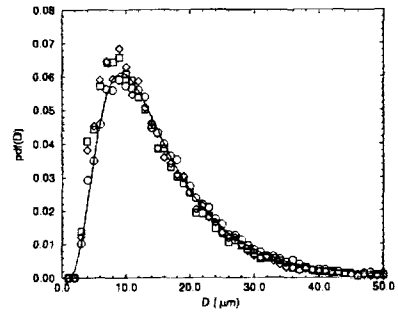


Figure 7: Probality density function for ○, $y = -30$; □, 0; ◇, 30 mm, — log-normal fit for y=-30mm. x=156 cm, stable stratified case.

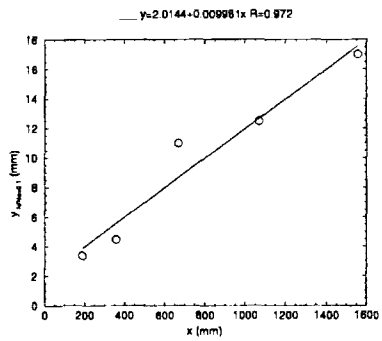


Figure 8: Upper limit of the diffusion zone for droplets of size, $10 < D < 15\,\mu m$.

## 3.1 Results

Two sets of experiments were conducted to systematically study the role of gravity. In all the experiments, only half of the wind tunnel entrance cross section was laden with uniform-concentration spray of droplets of a given polydispersed size distribution shown by the open circles in Fig. 4. In the first set, the uniform-concentration droplet spray initially occupied the lower half portion of the entrance cross section (stable stratified case), while in the second set the spray initially occupied the upper half portion of the wind tunnel cross section (unstable stratified case).

**Stably-stratified case**

The mean and fluctuations of the longitudinal and normal velocities are shown in Fig. 6; for clarity, only four bins are shown. One observes that, at $x = 67\,cm$ there is still a slight influence of the splitter wake. Indeed, around the position $y = 0\,mm$, there is a slight effect in the mean velocity and an increase in both fluctuating components of the velocity. Nevertheless, one can conclude that the flow is almost homogeneous turbulence with the value of $u'/U$ and $v'/U$ being close to those of the free stream, that is 2 and 1.4 respectively, giving a ratio $u'/v'$ of 1.4, close to the well known value of 1.2 reported for turbulent channel flow by Comte-Bellot and Corrsin [8]. The main point to note is the fact that no influence of the particles' sizes is observed on the fluctuations of the velocity, but for the smallest ones ($D < 5\mu m$) whose value is constant and equal to the value in the free stream. This fact is more clearly shown in Fig. 5 where profiles of the flux of particles across the probe volume (an indicator of the concentration of the droplets) are plotted according to their size. These profiles show two very distinct regions. The first one, where the flux is constant, corresponds to the free stream, and the second one where the particle turbulent diffusion has already carried the droplets from the droplet-laden free stream to the upper part of the channel with no droplets. One observes that the decrease of the mass flux is almost exponential, and more importantly that it is, to a first order approximation, the same for all droplets whatever their size (note that the three straight lines are parallel to each other). This is further confirmed in Fig. 7 where we show the size PDF of the droplets measured at three different vertical positions. All three distributions are seen to be almost identical, but for a small decrease in the number of big droplets resulting in a small increase of the PDF for small diameters when y increases.

As one can see in Fig. 4, this was not the case at downstream distances closer to the splitter plate where a difference in PDFs is observed. Indeed, one clearly

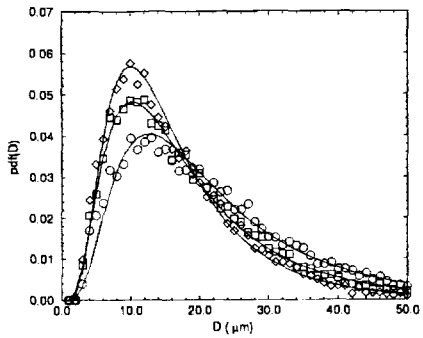


Figure 9: Probality density function for ∘, $y = -30$; □, 0; ⋄, 30 mm, — log-normal fit for y=30 mm. x=156 cm, unstable stratified case.

notes that small droplets are diffused in the upper part of the channel much faster than big ones resulting in an important increase of the PDF for small diameters when y increases. The large scale eddies structure of the wake is responsible for this effect. The rate of diffusion of droplets in the upper half of the channel can be measured from the data shown in Fig. 5. The upper limit can indeed be defined as the location where the data rate has fallen below a certain threshold. Normalizing these curves by the data rate in the free stream, $N_o$, and using a definition similar to that used in boundary layers, the upper limit of the diffusion zone has been chosen to be the location where the normalized data rate, $N/N_o$, is 0.1. The result obtained for particles of size $10 < D < 15\,\mu m$, representative of the spray, is shown in Fig. 8. One observes that this evolution is almost linear with a growth rate of 1%, a value very close to the measured normal turbulent intensity, $v'/U$, of 1.4%.

**Unstably-stratified case**

Similar measurements have been carried out where the injection of droplets was done in the upper half of the channel. In this second case the diffusion process is in the same direction as the gravity. Figure 9 shows three PDF taken across the test section. One clearly observes that big droplets are diffused in the lower part at a much larger rate than small ones. This can be seen from the widening of the distribution when descending from $y = 30\,mm$ to $y = -30\,mm$. Measurements are currently in progress to obtain a better understanding of the difference that exists between the stable and unstable, the marked difference observed in the PDFs cannot be explained with the simple linear addition of the settling velocity of the droplets which is less than $0.1\,m/s$ in all cases. Additionnal similar measurements are underway with a vertical splitter plate in order to separate diffusion effects from gravity effects.

**Acknowledgements** This research has been supported by NASA grant NAG3-1831.

# References

[1] C.T.Crowe, T.R.Troutt and J.N.Chung, "Numerical models for two-phase turbulent flows", Ann. Rev. Fluid Mech. **28**, 11 (1996).

[2] S.E.Elghobashi, "On predicting particle-laden turbulent flows", App. Sci. Res. **52**, 309 (1994).

[3] S.E.Elghobashi and T.W.Abou-Arab, "A two-equation turbulence model for two-phase flows", Phys. Fluids **26**, 931 (1983).

[4] J.K.Eaton and J.R.Fessler, "Preferential concentration of particles by turbulence", Int. J. Multiphase Flow **20**, Suppl., 169 (1994).

[5] L.-P.Wang and M.R.Maxey, "Settling velocity and concentration distribution of heavy particles in homogeneous isotropic turbulence", J. Fluid Mech. **256**, 27 (1993).

[6] S.E.Elghobashi and G.C.Truesdell, "On the two-way interaction between homogeneous turbulence and dispersed solid particles. I: Turbulence modification", Phys. Fluids A**5**, 1790 (1993).

[7] O.A.Druzhinin and S. Elghobashi, "Direct numerical simulations of bubble-laden turbulent flows using the two-fluid formulation", Phys. Fluids **10**, 685-697 (1998).

[8] G. Comte-Bellot and S. Corrsin, "Isotropy of grid generated turbulence" J. Fluid Mech.**25**, 657-682 (1966).

[9] K. T. Kiger, "Particle Dispersion and Inter-Phase Kinetic Enery Transfer in a Turbulent Two-Phase Shear Layer" PhD. Dissertation, University of California San Diego (1995).

[10] B.J. Lazaro and J.C. Lasheras, "Particle Dispersion in the developing Shears Layer. Part I" J. Fluid Mech. **235**, 143-178 (1992).

[11] B.J. Lazaro and J.C. Lasheras, 1992 "Particle Dispersion in the developing Shears Layer. Part II" J. Fluid Mech. **235** 143-178 (1992).